I&EC research
Industrial & Engineering Chemistry Research

Article

Cite This: Ind. Eng. Chem. Res. 2018, 57, 4505−4513

pubs.acs.org/IECR

Deactivation Mechanism and Regeneration Study of Ga−Pt Promoted HZSM-5 Catalyst in Ethane Dehydroaromatization

Xinwei Bai,[†] Anupam Samanta,[†] Brandon Robinson,[†] Lili Li,*[,‡] and Jianli Hu*[,†]

[†]Department of Chemical and Biomedical Engineering, Center for Innovation in Gas Research and Utilization, West Virginia University, Morgantown, West Virginia 26506, United States

[‡]School of Life Science and Agriculture, Zhoukou Normal University, Zhoukou 466000, China

Supporting Information

ABSTRACT: Direct nonoxidative conversion of ethane to aromatics has become an effective way of upgrading shale gas. Metal-promoted shape selective zeolite catalysts are often used for aromatization. Although the coking issue of the catalysts in ethane aromatization has been reported, the deactivation mechanism and the performance of regenerated Ga−Pt promoted HZSM-5 needs to be further investigated. The objective of this study is to elucidate deactivation mechanism of Ga−Pt promoted HZSM-5 and investigate the feasibility of regenerating deactivated catalysts for commercial viability. When using lower concentration of oxygen (2 vol %) for regeneration, decreased catalyst deactivation rate was observed. The metal particle size, crystalline structures, and acidity are characterized by various analytical instrumentations (TEM, XRD, NH_3-TPD). The change of Bronsted acidity was observed on regenerated catalysts. The results showed that metal agglomeration and leaching of Pt from homogeneous Ga−Pt particle were the main causes of deactivation other than coke deposition, indicating that stabilization of bimetallic metal particles on zeolite surface is critical.

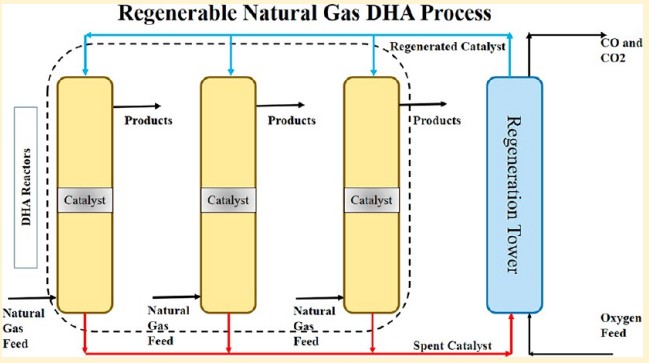

1. INTRODUCTION

Aromatic compounds are important basic chemical intermediates in the production of synthetic materials such as nylon and polyurethane. Currently, the aromatic hydrocarbons are primarily obtained from petroleum refining processes. For example, catalytic reforming of *n*-heptane, cyclohexane, paraffins, extraction of aromatics from refinery naphtha and coal tar distillation.[1−12] Ethane is one of the most important constituents in shale gas and some shale gas reservoirs contain over 20% of ethane and propane.[13] In past decades, indirect natural gas conversion via syngas was widely applied in industry.[14−16] However, indirect reaction pathway requires higher capital investment, which makes direct shale gas conversion routes attractive.[17] Although direct natural gas catalytic conversion to higher value chemicals has been studied for several decades, it has not been commercialized due to the poor process performance and stability of the catalysts.[18−20]

Zeolites have been developed for many decades and they have enormous potential in converting natural gas into higher value chemicals such as acetaldehyde, aromatics, and dimethyl ether.[21−26] Particularly, HZSM-5 zeolite is widely used in catalytic natural gas dehydroaromatization (DHA) due to its acidic and shape selective properties.[27] Methane, as a major component in shale gas, is widely studied in catalytic DHA.[18,20] However, compare to ethane, direct methane DHA requires higher reaction temperature and sometimes requires other pretreatment such as nonthermal plasma activation, to achieve higher aromatic yield.[28,29] With the difficulty in direct methane DHA, there is promising research focusing on direct ethane DHA. Krogh et al.[30] used Re/HZSM-5 to achieve 65% aromatic selectivity under 550 °C. Chetina et al.[31] discovered that platinum and gallium doped HZSM-5 catalyst can achieve 64% aromatic selectivity under 550 °C.

Catalyst deactivation can be one of the most striking issues in scientific research and industry application. According to our previous experimental results, in direct DHA, deactivation was severe when transition metal doped zeolite catalysts were used.[32] Literature reports showed that coke deposit which occupied the external surface or zeolite channels was the main cause of catalyst deactivation of the catalyst.[33−35] To maintain the stability of the catalyst, attempts have been made by adding additives such as carbon monoxide, carbon dioxide and steam to remove the carbon coke produced.[36−38] Some researchers have been investigating deactivation and regeneration of catalysts for methane DHA. Chen et al.[39] reported that the deactivation of Mo/HZSM-5 was due to the formation of carbon nanotube which caused leaching of Mo from the zeolite

Received: December 11, 2017
Revised: March 18, 2018
Accepted: March 21, 2018
Published: March 21, 2018

ACS Publications © 2018 American Chemical Society

DOI: 10.1021/acs.iecr.7b05094
Ind. Eng. Chem. Res. 2018, 57, 4505−4513

surface. Ma et al.[40] used nitrogen monoxide additive to study the catalyst regeneration mechanism. Based on our previous study,[32] gallium−platinum promoted HZSM-5 catalyst exhibited improved performance in ethane DHA as compared with Mo-HZSM-5. This is largely because the presence of platinum facilitates dehydrogenation of ethane, accelerating the formation of ethylene which is an important intermediate in ethane aromatization reaction However, the deactivation mechanism and regeneration study for the gallium−platinum bimetallic zeolite catalyst are still lacking. We have not seen any literature reports that discuss regeneration strategy as practiced in refining industry.

Catofin is a commercialized propane dehydrogenation process which consists of eight reactors in swing operation. For each reactor, the catalytic reaction time is 8 min and subsequently, the catalyst is regenerated via oxidative coke removal.[41,42] Inspired by this commercialized process, this study is focused on investigating the feasibility of cyclic regeneration as practiced in Catofin. The DHA reaction is set for 15 min before switching to regeneration mode. Based on our previous publication,[32] metal doped ZSM-5 catalyst containing 2.5 wt % of gallium and 0.5 wt % of platinum exhibited good performance in ethane dehydroaromatization because platinum facilitates the formation of ethylene which is an important intermediate in this reaction. In this study, this catalyst system is further investigated and the analysis is focused on elucidating deactivation mechanism and developing regeneration processes for Ga−Pt promoted HZSM-5 catalyst in ethane DHA. The ultimate goal is to develop catalyst formulation strategy and regeneration process that, by combining both approaches, a commercially viable DHA technology can be developed. It is anticipated that commercial ethane DHA process could be designed in swing operation mode. As a result, the impacts of the variation of regeneration process parameters, such as oxygen concentration, temperature, and cycle time, on the regeneration performance of the Pt−Ga/HZSM-5 catalyst are investigated. This study is focused on elucidating deactivation mechanism via correlation of surface characterization results with process performance data.

2. EXPERIMENTAL SECTION

2.1. Preparation of Ga−Pt/ZSM-5 Catalysts. The gallium−platinum bimetallic zeolite catalyst containing 2.5 wt % of gallium and 0.5 wt % of platinum was prepared by incipient wetness technique. ZSM-5 zeolite with SiO_2/Al_2O_3 molar ratio (SAR) of 50 was used for catalyst preparation. NH_4-ZSM-5 was supplied by Zeolyst Inc. Proton-type H-ZSM-5 was prepared by calcining NH_4-ZSM-5 at 500 °C in air for 3 h. The obtained H-ZSM-5 was impregnated with the mixture of gallium nitrate hydrate and chloroplatinic acid hexahydrate aqueous solution and dried in an oven at 100 °C for 12 h. Finally, the dried material was calcined in air at 550 °C for 4 h.

2.2. Catalyst Characterization. The metal particle size and composition were characterized by a transmission electron microscope (JEOL, JEM-2100). The specimen was prepared by sonicating the suspension of the sample in isopropanol. The operating voltage was 200 kV. Meanwhile, the energy dispersive X-ray spectroscopy (EDX) analysis was performed for each sample. Powder X-ray diffraction (XRD) was performed on a PANalytical X'Pert Pro X-ray Diffractometer under 45 kV and 40 mA. The scanning angle ranged from 5° to 85°.

2.3. Experimental Setup. The reaction was carried out in Micromeritics Autochem 2950 analyzer connected to a mass spectrometer. For each experiment, 100 mg of catalyst were loaded into a quartz tube reactor. Reaction was carried out under atmospheric pressure and continuous flow conditions. The catalyst was heated to 650 °C in helium at a flow rate of 50 mL/min with the heating rate of 10 °C/min. The catalyst temperature was kept at 650 °C for 60 min. The feedstock used in DHA reaction consisted of 20 vol % of ethane and 80 vol % of helium. Total flow rate was set at 50 mL/min. After 15 min of reaction, helium was introduced to purge the ethane in the system, and the catalyst was cooled to 500 °C for regeneration in the presence of 10 vol % or 2 vol % of oxygen in helium. When 10 vol % of oxygen was used, the regeneration time was 60 min, whereas when using 2 vol % of oxygen, the regeneration time was 120 min to ensure maximum coke removal, while the outlet carbon dioxide level was monitored by Pfeiffer Omnistar mass spectrometer. After catalyst regeneration, helium was introduced to purge the remaining oxygen in the system and the catalyst was heated to 650 °C at ramping rate of 10 °C/min for next DHA reaction cycle. A total of five DHA cycles (one fresh and four regenerated) were performed for each catalytic reaction. The DHA reaction products were analyzed by Pfeiffer Omnistar mass spectrometer. To ensure consistency between runs, for each cycle, $t = 0$ is set at the point when aromatics production during the induction period reached at maximum.

Temperature-programmed oxidation (TPO) and ammonia temperature-programmed desorption (NH_3-TPD) were performed in Micromeritics Autochem 2950 analyzer using 2 vol % of oxygen and 15 vol % of ammonia, respectively. A thermoconductivity (TCD) detector was employed to record the signal which reflects the composition change of the outlet during TPO and TPD experiments. The spent catalyst sample was heated to 150 °C to remove the moisture, after which the temperature was programmed to 700 °C at a rate of 2 °C/min. The temperature was held at 700 °C for 30 min. For TPD, the sample was heated to 700 °C at a rate of 5 °C/min. In addition, a TA Instrument SDT 650 thermogravimetric analysis (TGA) unit was used to quantify the amount of coke on the catalyst. The flow rate of feed gas containing 5 vol % oxygen in helium was set at 20 mL/min. In TGA analysis, around 25 mg of the spent catalyst sample was heated to 150 °C and held for 30 min to ensure complete moisture removal. Then the temperature was raised to 700 °C at the rate of 5 °C/min. The temperature was held at 700 °C for 120 min for complete coke removal.

3. RESULT AND DISCUSSION

Each DHA reaction cycle was carried out for 15 min before switching to regeneration mode. The regeneration was carried out using either 2 vol % or 10 vol % oxygen. Volumetric flow rates of products were measured to compare the performance among regeneration cycles. Figures 1 and 2 show time-on-stream volumetric flow rate of hydrogen, benzene and toluene at reactor outlet under the regeneration conditions of using 2 vol % and 10 vol %, respectively. For each oxygen concentration, four catalyst regeneration cycles were carried out. Supporting Information (SI) Tables S1−S3 summarize quantitatively the change of productivity of these three products within single cycle and between cycles. Essentially, SI Tables S1−S3 are numerical description of Figures 1-2, where the percentage change of productivity within each cycle and between cycles are calculated. Figures 1 and 2 show that the catalyst regenerated after first fresh run exhibits better performance in producing aromatic products. The details will

DOI: 10.1021/acs.iecr.7b05094
Ind. Eng. Chem. Res. 2018, 57, 4505−4513

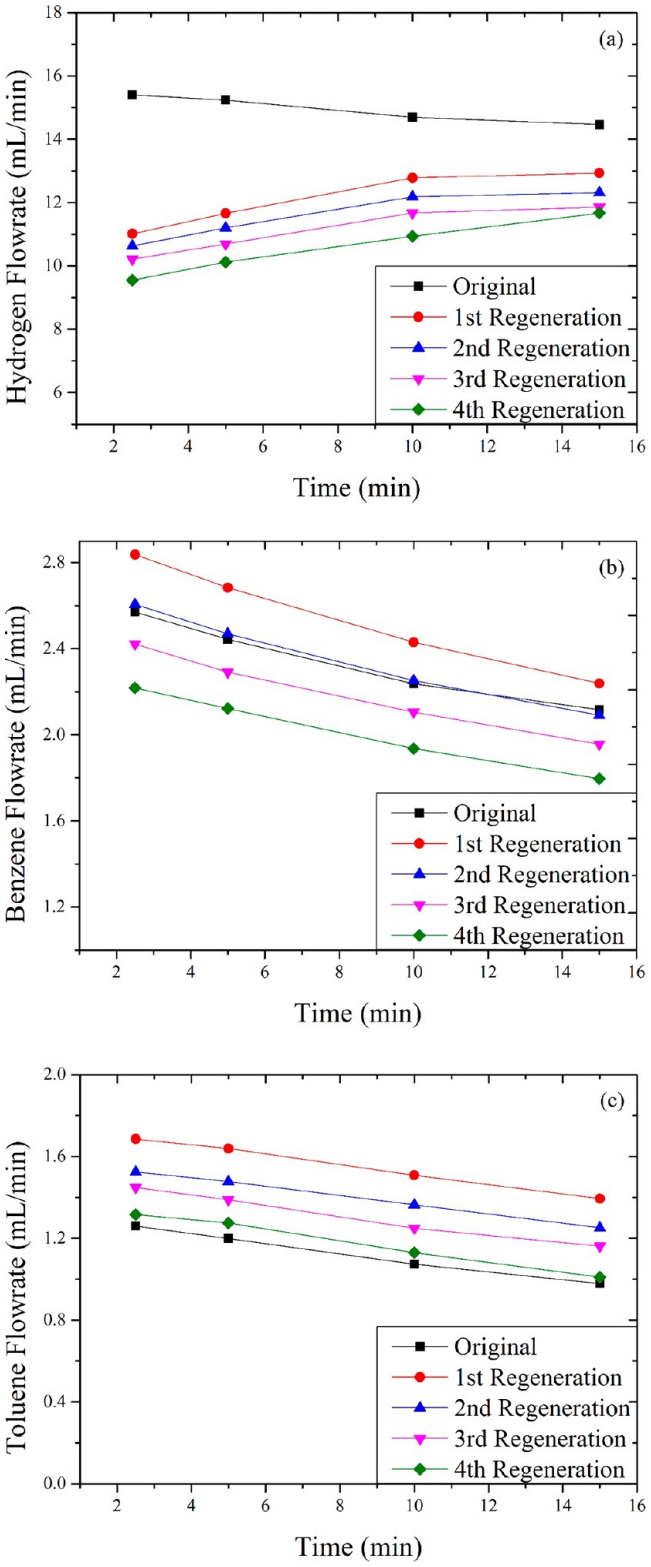

Figure 1. Production of (a): hydrogen, (b): benzene, (c): toluene using 10% of oxygen for catalyst regeneration, 15 min of DHA reaction.

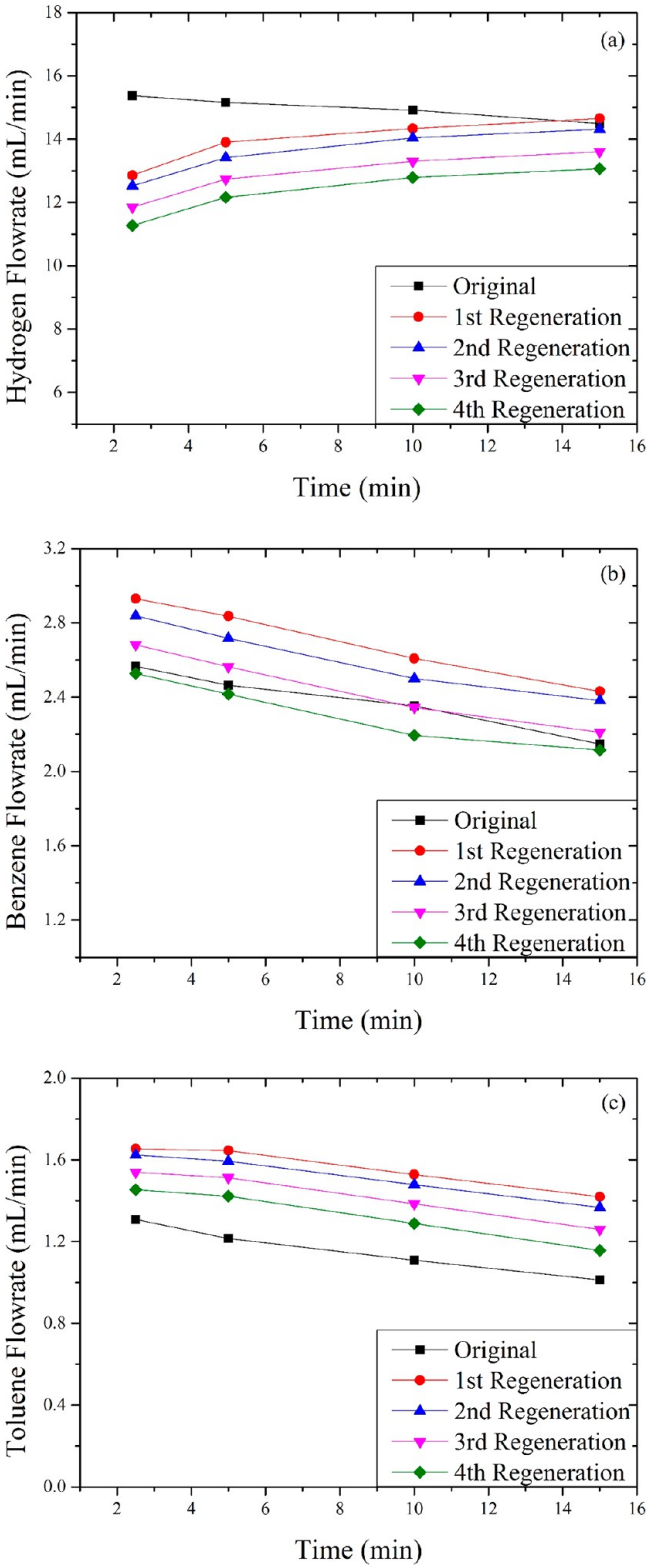

Figure 2. Production of (a): hydrogen, (b): benzene, (c): toluene using 2% of oxygen for catalyst regeneration, 15 min of DHA reaction.

be discussed later in this section. As shown in SI Table S2, when the catalyst is regenerated by using 10 vol % oxygen, in each reaction cycle, benzene concentration at outlet decreases at a range of 19.0% to 21.0% after 15 min time-on-stream. A similar trend was observed on toluene concentration at reactor outlet, dropping in a range of 17.2% to 22.2%. In contrast, when using 2 vol % oxygen for catalyst regeneration, the benzene production dropped in a range of 16.3% to 17.6% within a single cycle, and the toluene production dropped in a range of 14.2% to 22.6% (SI Table S3)

DOI: 10.1021/acs.iecr.7b05094
Ind. Eng. Chem. Res. 2018, 57, 4505−4513

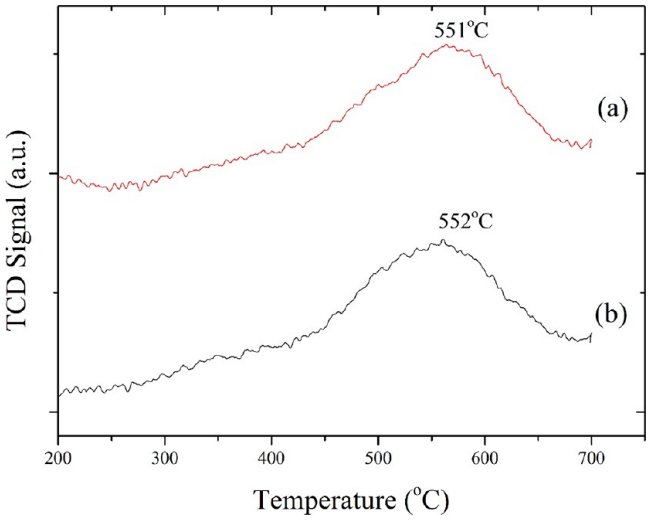

Figure 3. Temperature programming oxidation profiles of the spent catalyst sample using (a): 10 vol % of oxygen (b): 2 vol % of oxygen.

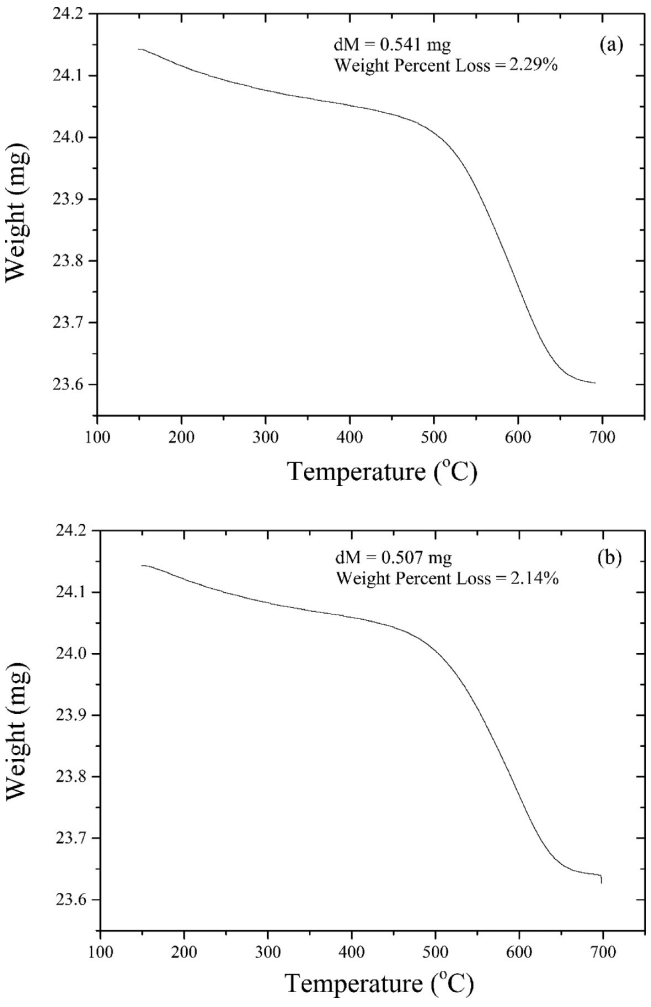

Figure 4. TGA curves of coke-containing spent Ga−Pt/ZSM-5 catalyst after fifth DHA reaction cycles: (a) regenerated by 10 vol % of oxygen (b) regenerated by 2 vol % of oxygen.

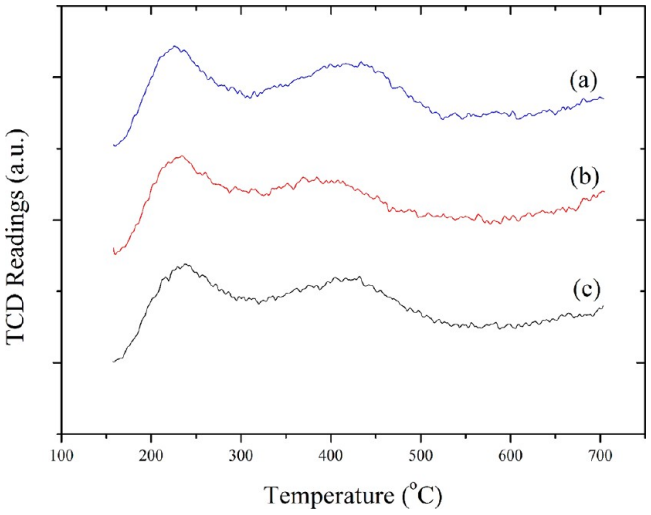

Figure 5. Ammonia temperature programming desorption profiles of (a): fresh catalyst and regenerated catalyst sample using (b): 10 vol % of oxygen (c): 2 vol % of oxygen.

Table 1. Numerical Ammonia Temperature Programmed Desorption Result

	desorption temperature (°C)		$M_{ammonia}$ (mmol/g catalyst)		
	T_1	T_2	T_1	T_2	M_{total} (mmol/g catalyst)
fresh catalyst	225.9	430.0	0.173	0.190	0.363
regenerated by 10 vol % O_2	233.8	390.9	0.182	0.179	0.362
regenerated by 2 vol % O_2	238.6	416.5	0.184	0.181	0.365

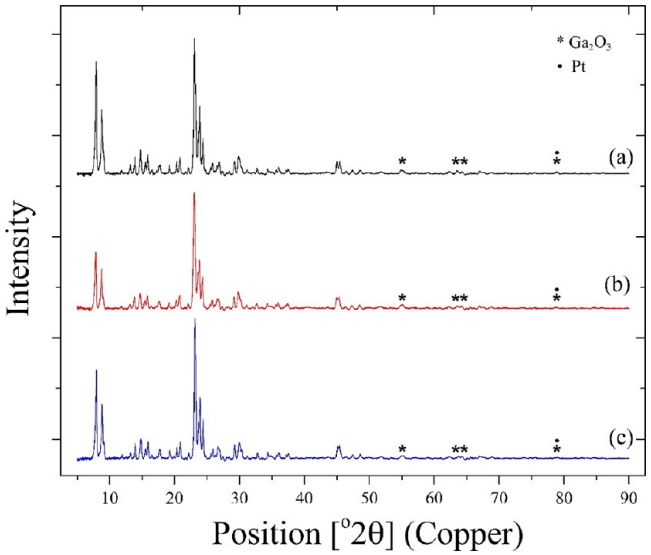

Figure 6. X-ray diffraction patterns of Ga−Pt/ZSM-5 catalyst: (a) fresh catalyst, (b) spent sample after five DHA reaction cycles, regenerated by 10 vol % of oxygen, coke removed (c) spent sample after five DHA reaction cycles, regenerated by 2 vol % of oxygen, coke removed.

Figure 2 shows the reactivity of the Ga−Pt/ZSM-5 catalyst with 15 min on-stream time, and the catalyst was regenerated using 2 vol % of oxygen. Compared with the conditions of using 10 vol % of oxygen for regeneration, within a single cycle, catalyst deactivation rate appears to be reduced. That is, the loss of productivity in a single cycle is less when using 2 vol %

DOI: 10.1021/acs.iecr.7b05094
Ind. Eng. Chem. Res. 2018, 57, 4505−4513

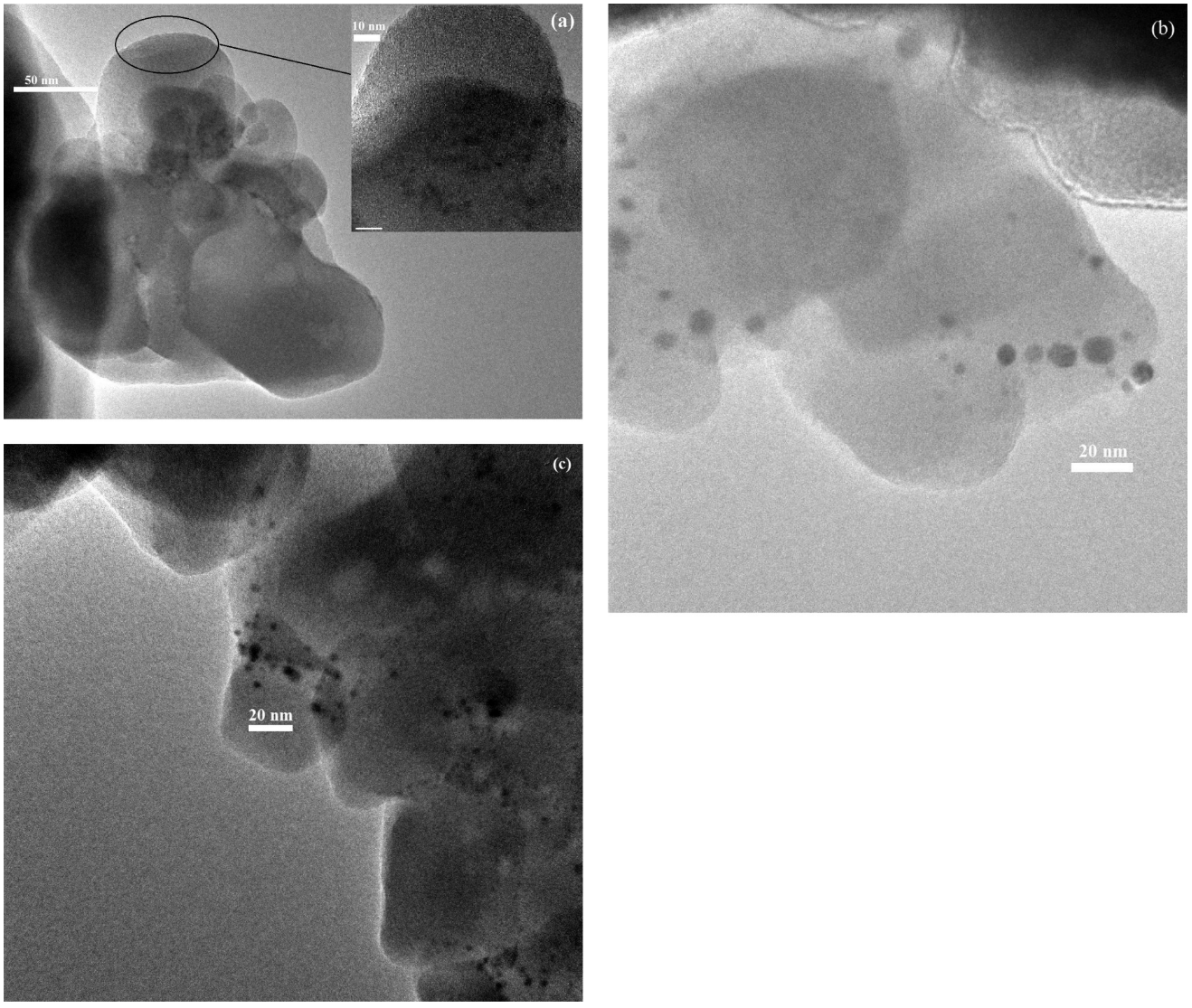

Figure 7. TEM image of Ga−Pt/ZSM-5 samples: (a) fresh catalyst, (b) spent catalyst with coke, after five regeneration cycles using 10 vol % oxygen (c) spent catalyst with coke, after five regeneration cycles using 2 vol % oxygen.

oxygen for regeneration. Compare the aromatic production among cycles, the result shows that the loss of activity between cycles is much less for 2 vol % oxygen regeneration. Therefore, using lower oxygen concentration to regenerate the catalyst can decrease the deactivation rate of the catalyst.

TPO results are shown in Figure 3. For both samples, the only peak identified is around 550 °C which indicates that the maximum coke oxidation rate occurs at that temperature. Per suggestion from zeolite supplier, Zeolyst Inc., NH_4^+ form ZSM-5 was calcinated at 550 °C during catalyst preparation. We have evaluated catalyst regeneration conditions by searching the literature. It is well-known that coke oxidation process is highly exothermic which generates "hot spots" in the catalyst. Because these hot spots are located underneath the coke, the temperature could be higher than measured. The potential damage of the structure of the zeolite could take place. In a research paper by Gao et al.,[43] for Mo-promoted ZSM-5, they selected regeneration at 500 °C. Referring to Gao's work, and with the consideration that localized surface temperature may exceed 550 °C due to the presence of hot spots, we have chosen 500 °C as oxidation temperature for catalyst regeneration in the presence of 2 and 10 vol % O_2.

TGA experiment was carried out to quantify the amount of the coke after five 15 min-reaction cycles. As shown in Figures 3 and 4, with the increase of the temperature, the coke was oxidized by the oxygen feed and the maximum weight loss occurs at around 550 °C, which reflects our previous TPO result. Subtracting the initial spent catalyst weight (moisture removed) from the ending weight, it shows that both of the catalyst has similar amount of the coke in the catalyst. Therefore, the amount of coke accumulated is not a factor causing the performance difference.

An NH_3-TPD analysis has been performed and the result is shown in Figure 5 and peak information is shown in Table 1. NH_3-TPD indicates different acid sites (Lewis and Bronsted acid sites) and their strength in fresh and regenerated catalyst. The peak appears at lower temperature (T_1) is identified as Lewis acid sites and the other peak (T_2) is identified as Bronsted acid sites.[20,44] When the zeolite was received from Zeolyst Inc., it was in ammonium form that can be expressed as Al− $O(NH_4)^+$−Si. Upon calcination at 550 °C, the ammonium

DOI: 10.1021/acs.iecr.7b05094
Ind. Eng. Chem. Res. 2018, 57, 4505−4513

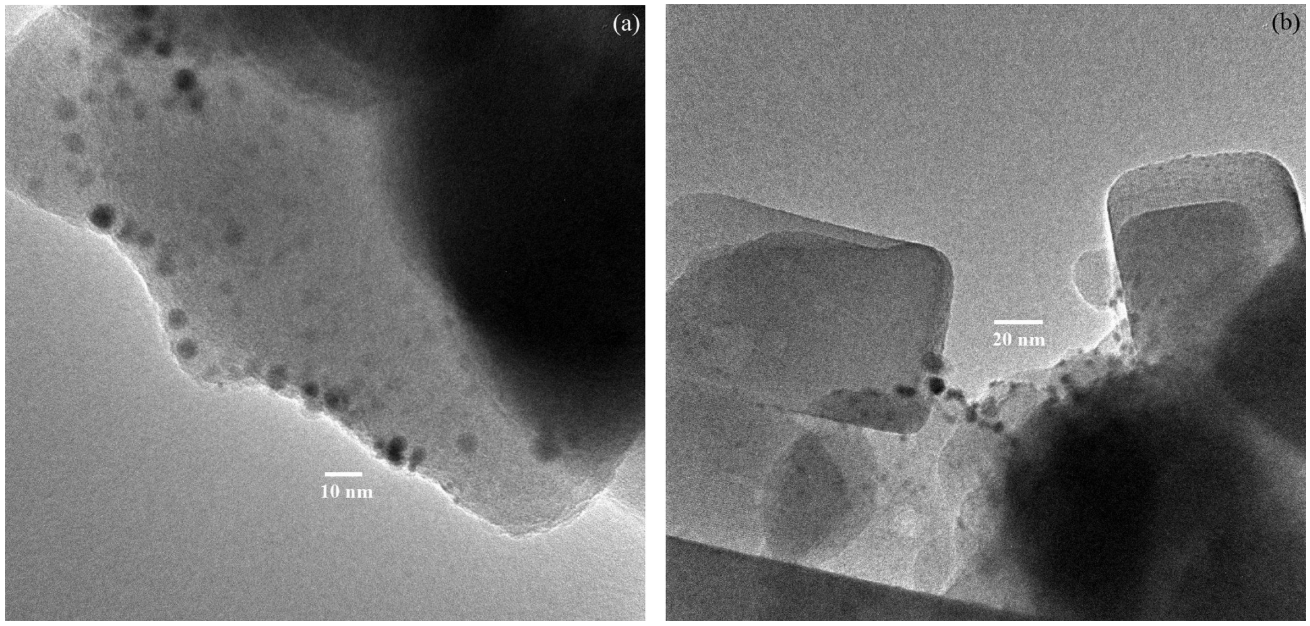

Figure 8. TEM image of regenerated Ga−Pt/ZSM-5 samples: (a) coke-removed spent catalyst after five regeneration cycles using 10 vol % oxygen (b) coke-removed spent catalyst after five regeneration cycles using 2 vol % oxygen.

Table 2. EDX Result of Surface Particles of Fresh and Coke-Removed Spent Ga−Pt/ZSM-5 Catalysts

elements	fresh catalyst	regenerated by 10 vol % O_2	regenerated by 2 vol % O_2
gallium (atomic %)	0.74	1.13	1.41
platinum (atomic%)	0.15	4.99	3.06

Table 3. EDX Result of Surface Particles of Spent Ga−Pt/ZSM-5 Catalysts with Coke

elements	regenerated by 10 vol % O_2	regenerated by 2 vol % O_2
gallium (atomic%)	2.82	1.05
platinum (atomic%)	5.65	2.15

form is transformed into bridge hydroxyl groups (Al−OH^+−Si) by releasing NH_3, forming the Bronsted acid sites.[44,45] It can be observed that the peak T_2 for regenerated catalysts shifts to a lower temperature indicating the decrease of Bronsted acid strength. The group postulates that the decrease in Bronsted acid strength in regenerated catalysts is due to dealumination of the catalyst during the reaction and regeneration.[45] Evidently, 10 vol % O_2 exhibited stronger impact on dealumination during regeneration process.

Figure 6 shows X-ray diffraction patterns of fresh and all spent catalyst samples from the experiments. The high intensity peaks between 8−9° and 20−25° indicate that both reaction and the regeneration process did not change the bulk crystallized structure of the zeolite (Figure 5a). These peaks are the characteristics of the structure of calcinated HZSM-5 zeolites. As shown in Figure 6b and 6c, the signals are observed at 55°, 63° to 65°, and 79°, which are ascribed to metals on zeolite. It was observed that at the range of 8° to 9°, the relative peak intensities of spent samples are lower than that obtained from the fresh catalyst sample. This could be caused by the presence of remaining coke on the spent catalyst.

TEM images of fresh and spent catalysts obtained at the end of five regeneration cycles without coke removal are shown in Figure 7. Two spent catalyst samples are generated from using 10 vol % oxygen and 2 vol % oxygen, respectively. As shown in Figure 7a, the metal particles of fresh catalyst can only be observed under high resolution camera and the particle size is generally between 2 and 4 nm. However, TEM of spent catalysts with or without coke removal (Figure 7b, c and Figure 8) showed the presence of metal nanoparticles of size from 3 to 10 nm. This increment of particle size was caused by metal sintering during reaction at high temperature (650 °C). TEM analysis indicates that most of the metal particles are residing outside the zeolite pore since average pore diameter of ZSM-5 is 5.5 Å only, whereas the size of metal particles is much larger (3−10 nm). As a result, metal sintering can cause not only loss of activity but also decrease in aromatic selectivity. The loss of aromatic selectivity is probably due to the inhibiting of shape selective property, such as channel blockage and acidity change.

From TEM EDX analysis of fresh catalyst, it is observed that the atomic ratio of Ga/Pt ranges from 4 to 5 throughout the material (Table 2). However, as shown in Table 3, in the selected areas, TEM EDX analysis of spent catalyst showed higher amount of Pt (2.15−5.65 atomic %) compared to Ga (1.05−2.85 atomic %) though the fresh catalyst contains higher amount of Ga (2.5 wt %) compared to Pt (0.5 wt %). The same trend is observed in regenerated catalyst (coke-removed sample), as shown in Table 3. This higher amount of Pt metal on selected areas manifests that Ga and Pt are not evenly distributed throughout the material of spent catalyst as compared to fresh catalyst. This indicates that metal particles shown in TEM images contain mostly Pt metal and less amount of Ga metal. This phenomenon is attributed to higher mobility of Pt nanoparticles on support at high temperature. Gallium metal in oxide form has strong interaction with the zeolite support compared to Pt. Due to the difference in metal−support interactions, the homogeneous meal distribution of fresh catalyst deteriorates at high reaction temperature. The Ga−Pt interaction is one of the essential factors that

DOI: 10.1021/acs.iecr.7b05094
Ind. Eng. Chem. Res. 2018, 57, 4505−4513

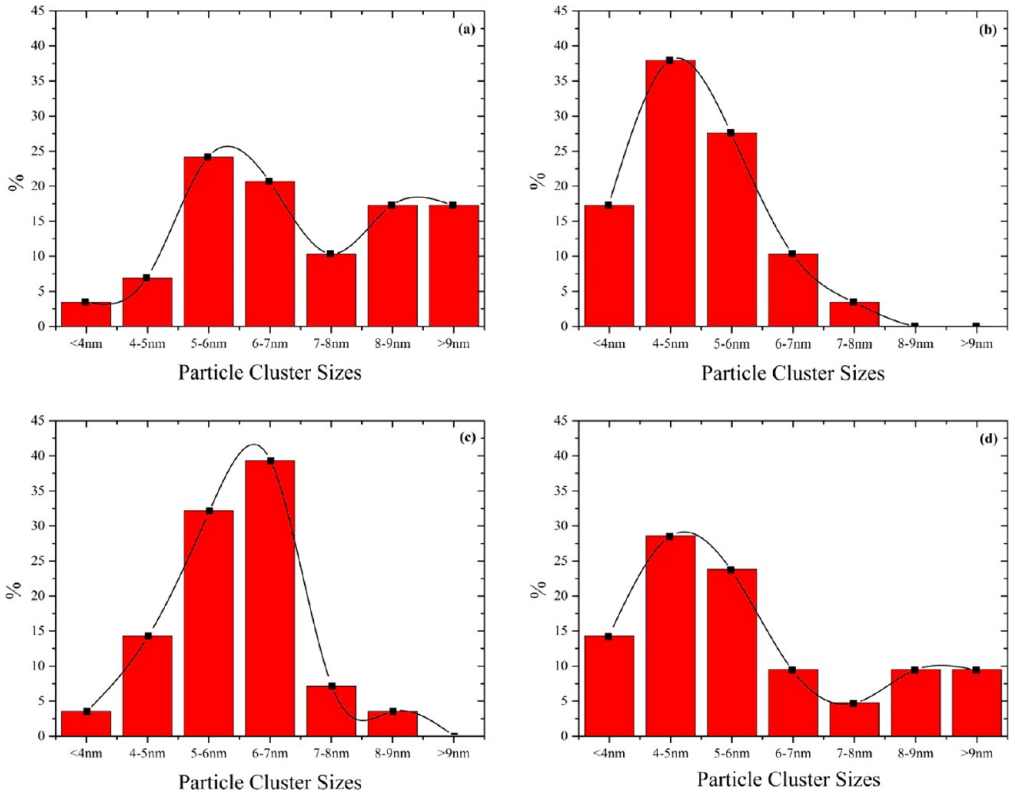

Figure 9. Particle size distribution of TEM images of various GaPt/ZSM-5 samples: (a) spent catalyst with coke, after five regeneration cycles using 10 vol % oxygen; (b) spent catalyst with coke, after five regeneration cycles using 2 vol % oxygen; (c) coke-removed spent catalyst after five regeneration cycles using 10 vol % oxygen; and (d) coke-removed spent catalyst after five regeneration cycles using 2 vol % oxygen.

impacts ethane conversion and aromatic selectivity. Due to the difference in migration ability, the interaction between these two metals through the alloy formation is affected. From TEM and EDX analysis of fresh and spent catalysts, it can be concluded that particle size increase and the change of metal nanoparticle composition are also important reasons for catalyst deactivation along with coke formation.

Figure 9 shows the general particle size in regenerated catalysts under different regeneration conditions. We found that when using higher concentration of oxygen to regenerate the catalyst, larger size metal particles are formed. In Figure 9, the size distribution of particle clusters shown in the TEM images was measured. The size of about and 28−30 particles was measured in each type of the sample. It is obvious that, when using higher concentration of oxygen in regeneration, metal particle agglomeration accelerates. This is mainly because coke oxidation rate becomes faster when using higher concentration of oxygen. Since the coke oxidation is highly exothermic, higher oxidation rate will generate more heat that is difficult to release, creating hot spots between coke and active sites (metals), therefore metal sintering becomes inevitable. This explains the trend of metal particle size during regeneration at different level of oxygen content. It is also noticed that the agglomerated particle clusters are easily identified in TEM samples after coke removal, implying that metal agglomeration process is irreversible under current oxidative regeneration conditions. There are other industrial processes where metal redispersion can be achieved. For example, oxychlorination process is used to redisperse Pt−Sn reforming catalyst.

In previous section, Figures 1 and 2, it has been noticed that the aromatic production of first regenerated samples were better than the fresh sample, this can be caused by the relocation of the metal particles inside the zeolite matrix during the oxidation process which changes the acidity of the catalyst. We will investigate this phenomenon in future study using in situ analytical techniques. For hydrogen production, there is a huge performance loss between first and second cycles in both samples. This can be explained by the hypothesis that after first regeneration, the production of hydrogen started to decrease due to the loss of metal surface area which is caused by agglomeration, as well as metal leaching from active sites. This could also explain that the decrease of production of benzene and toluene after second cycle. It is noticed that the density of surface particles appears to be less in samples regenerated using low oxygen concentration. This phenomenon could be associated with heat transfer limitation during coke removal, which increases the mobility of metal particles. With smaller metal particles and less severe agglomeration phenomenon, the catalyst which regenerated by lower oxygen concentration deactivates slower within a single DHA reaction cycle.

4. CONCLUSION

In DHA of ethane, the agglomeration is more severe in first DHA reaction cycle and the first regeneration step, which cause the dramatic loss of hydrogen productivity. According to TEM results, in additional to coke formation, the deactivation mechanism is speculated to follow the following mechanism: metal particles agglomeration and the particles migration toward the surface of the zeolite. Corresponding EDX results reveal that the agglomeration appears more likely to be heterogeneous by nature, which means that the gallium particles are surrounded by platinum particles which are

DOI: 10.1021/acs.iecr.7b05094
Ind. Eng. Chem. Res. 2018, 57, 4505−4513

subsequently leached out from the channel. Regeneration of the Ga−Pt/ZSM-5 catalyst using lower concentration of oxygen can improve the catalyst stability and decrease the rate of productivity loss after each regeneration cycle. NH_3-TPD result indicates that using higher concentration of oxygen in regeneration step can potentially accelerate the dealumination of the catalyst. Other than coke removal, our findings indicate that both catalyst stability and regeneration protocol are important in DHA reaction. New catalyst formulation strategy that incorporates coke inhibitors is necessary. Further study of regeneration technology and/or coke-formation inhibitor is recommended to make the direct natural gas DHA viable in future industrial application.

■ ASSOCIATED CONTENT

Supporting Information

The Supporting Information is available free of charge on the ACS Publications website at DOI: 10.1021/acs.iecr.7b05094.

Table S1−S3: numerical performance data for hydrogen, benzene and toluene production of different regeneration conditions (PDF)

■ AUTHOR INFORMATION

Corresponding Authors

*(L.L.) E-mail: 13672165360@163.com.
*(J.H.) E-mail: john.hu@mail.wvu.edu.

ORCID

Lili Li: 0000-0002-4247-4111
Jianli Hu: 0000-0003-3857-861X

Notes

The authors declare no competing financial interest.

■ ACKNOWLEDGMENTS

We acknowledge financial support from West Virginia Higher Education Policy Commission under grant number HEPC.dsr.18.7

■ REFERENCES

(1) Hamoule, T.; Peyrovi, M. H.; Rashidzadeh, M.; Toosi, M. R. Catalytic Reforming of N-Heptane over Pt/Al-HMS Catalysts. *Catal. Commun.* **2011**, *16* (1), 234.

(2) Li, J.; Chai, Y.; Liu, B.; Wu, Y.; Li, X.; Tang, Z.; Liu, Y.; Liu, C. The Catalytic Performance of Ni_2P/Al_2O_3 Catalyst in Comparison with Ni/Al_2O_3 Catalyst in Dehydrogenation of Cyclohexane. *Appl. Catal., A* **2014**, *469*, 434.

(3) Rahimpour, M. R.; Vakili, R.; Pourazadi, E.; Iranshahi, D.; Paymooni, K. A Novel Integrated, Thermally Coupled Fluidized Bed Configuration for Catalytic Naphtha Reforming to Enhance Aromatic and Hydrogen Productions in Refineries. *Int. J. Hydrogen Energy* **2011**, *36* (4), 2979.

(4) Rahimpour, M. R.; Jafari, M.; Iranshahi, D. Progress in Catalytic Naphtha Reforming Process: A Review. *Appl. Energy* **2013**, *109*, 79−93.

(5) Speight, J. G. *The Chemistry and Technology of Petroleum*, 5th ed.; CRC Press: Boca Raton, 2014.

(6) Wiatowski, M.; Kapusta, K.; Stańczyk, K. Analysis and Characteristics of Tars Collected during a Pilot-Scale Underground Coal Gasification (UCG) Trial. *Fuel* **2017**, *208*, 595.

(7) Tian, B.; Qiao, Y.; Bai, L.; Liu, F.; Tian, Y.; Xie, K. Separation and Structural Characterization of Groups from a High-Volatile Bituminous Coal Based on Multiple Techniques. *Fuel Process. Technol.* **2017**, *159*, 386.

(8) Tian, B.; Qiao, Y.; Bai, L.; Feng, W.; Jiang, Y.; Tian, Y. Pyrolysis Behavior and Kinetics of the Trapped Small Molecular Phase in a Lignite. *Energy Convers. Manage.* **2017**, *140*, 109.

(9) Xue, J.; Liu, G.; Niu, Z.; Chou, C. L.; Qi, C.; Zheng, L.; Zhang, H. Factors That Influence the Extraction of Polycyclic Aromatic Hydrocarbons from Coal. *Energy Fuels* **2007**, *21* (2), 881.

(10) Meng, X.; Gao, M.; Chu, R.; Miao, Z.; Wu, G.; Bai, L.; Liu, P. Construction of a macromolecular structural model of Chinese lignite and analysis of its low-temperature oxidation behavior. *Chin. J. Chem. Eng.* **2017**, *25* (9), 1314−1321.

(11) Lapidus, A. L.; Dergachev, A. A.; Kostina, V. A.; Silakova, A. A. Ethane Aromatization on Ga-Pt Pentasil Zeolites. *Pet. Chem.* **2008**, *48* (2), 83.

(12) Tian, B.; Qiao, Y.; Fan, J.; Bai, L.; Tian, Y. Coupling Pyrolysis and Gasification Processes for Methane-Rich Syngas Production: Fundamental Studies on Pyrolysis Behavior and Kinetics of a Calcium-Rich High-Volatile Bituminous Coal. *Energy Fuels* **2017**, *31* (10), 10665.

(13) Lutz, M. "A Bakken Producers Regional View on Gas & NGL Markets···". Available: http://www.platts.com/IM.Platts.Content/ProductsServices/ConferenceandEvents/2013/pc318/presentations/Michael_Lutz.pdf.

(14) Holmen, A. Direct Conversion of Methane to Fuels and Chemicals. *Catal. Today* **2009**, *142* (1−2), 2.

(15) Spivey, J. J.; Hutchings, G. Catalytic Aromatization of Methane. *Chem. Soc. Rev.* **2014**, *43* (3), 792.

(16) Horn, R.; Schlögl, R. Methane Activation by Heterogeneous Catalysis. *Catal. Lett.* **2015**, *145*, 23.

(17) Lunsford, J. H. Catalytic Conversion of Methane to More Useful Chemicals and Fuels: a Challenge for the 21st Century. *Catal. Today* **2000**, *63*, 165.

(18) Skutil, K.; Taniewski, M. Some Technological Aspects of Methane Aromatization (Direct and via Oxidative Coupling). *Fuel Process. Technol.* **2006**, *87* (6), 511.

(19) Karakaya, C.; Kee, R. J. Progress in the Direct Catalytic Conversion of Methane to Fuels and Chemicals. *Prog. Energy Combust. Sci.* **2016**, *55*, 60−97.

(20) Abdelsayed, V.; Shekhawat, D.; Smith, M. W. Effect of Fe and Zn Promoters on Mo/HZSM-5 Catalyst for Methane Dehydroaromatization. *Fuel* **2015**, *139*, 401.

(21) Liu, J.; Yu, L.; Zhao, Z.; Chen, Y.; Zhu, P.; Wang, C.; Luo, Y.; Xu, C.; Duan, A.; Jiang, G. Potassium-Modified Molybdenum-Containing SBA-15 Catalysts for Highly Efficient Production of Acetaldehyde and Ethylene by the Selective Oxidation of Ethane. *J. Catal.* **2012**, *285* (1), 134.

(22) Yakerson, V. I.; Vasina, T. V.; Lafer, L. I.; Sytnyk, V. P.; Dykh, G. L.; Mokhov, A. V.; Bragin, O. V.; Minachev, K. M. The Properties of Zinc and Gallium Containing Pentasils - The Catalysts for the Aromatization of Lower Alkanes. *Catal. Lett.* **1989**, *3* (4), 339.

(23) Steinberg, K. H.; Mroczek, U.; Roessner, F. Aromatization of Ethane on Platinum Containing ZSM-5 Zeolites. *Appl. Catal.* **1990**, *66* (1), 37.

(24) Deng, J.; Zhang, G.; Dong, S.; Pan, H.; Wang, H. Acidic Properties of ZSM-5 Zeolite and Conversion of Ethanol to Diethyl Ether. *Appl. Catal.* **1988**, *41* (C), 13.

(25) Chu, R.; Hou, W.; Meng, X.; Xu, T.; Miao, Z.; Wu, G.; Bai, L. Catalytic Kinetics of Dimethyl Ether One-Step Synthesis over CeO_2-CaO-Pd/HZSM-5 Catalyst in Sulfur-Containing Syngas Process. *Chin. J. Chem. Eng.* **2016**, *24* (12), 1735.

(26) Chu, R.; Song, C.; Hou, W.; Meng, X.; Miao, Z.; Li, X.; Wu, G.; Wan, Y.; Bai, L. Improved Stability of Pd/HZSM-5 Bifunctional Catalysts by the Addition of Promoters (CeO_2, CaO) for the One-Step Synthesis of Dimethyl Ether from Sulfur-Containing CO_2 Hydrogenation. *J. Taiwan Inst. Chem. Eng.* **2017**, *80*, 1.

(27) Guisnet, M.; Magnoux, P.; Canaff, C. Formation and Nature of Coke Deposits on Zeolites HY and HZSM-5. *Stud. Surf. Sci. Catal.* **1986**, *28*, 701−707.

DOI: 10.1021/acs.iecr.7b05094
Ind. Eng. Chem. Res. 2018, 57, 4505−4513

(28) Wang, L.; Tao, L.; Xie, M.; Xu, G.; Huang, J.; Xu, Y. Dehydrogenation and Aromatization of Methane under Non-Oxidizing Conditions. *Catal. Lett.* **1993**, *21* (1−2), 35.
(29) Li, X. S.; Shi, C.; Xu, Y.; Zhang, X. L.; Wang, K. J.; Zhu, A. M. Pulsed Streamer Discharge Plasma over Ni/HZSM-5 Catalysts for Methane Conversion to Aromatics at Atmospheric Pressure. *Plasma Processes Polym.* **2007**, *4* (1), 15.
(30) Krogh, A.; Hagen, A.; Hansen, T. W.; Christensen, C. H.; Schmidt, I. Re/HZSM-5: A New Catalyst for Ethane Aromatization with Improved Stability. *Catal. Commun.* **2003**, *4* (12), 627.
(31) Chetina, O. V.; Vasina, T. V.; Lunin, V. V. Aromatization of Ethane over Pt,Ga/HZSM-5 Catalyst and the Effect of Intermetallic Hydrogen Acceptor on the Reaction. *Appl. Catal., A* **1995**, *131* (1), 7.
(32) Samanta, A.; Bai, X.; Robinson, B.; Chen, H.; Hu, J. Conversion of Light Alkane to Value-Added Chemicals over ZSM-5/Metal Promoted Catalysts. *Ind. Eng. Chem. Res.* **2017**, *56* (39), 11006−11012.
(33) Bjørgen, M.; Svelle, S.; Joensen, F.; Nerlov, J.; Kolboe, S.; Bonino, F.; Palumbo, L.; Bordiga, S.; Olsbye, U. Conversion of Methanol to Hydrocarbons over Zeolite H-ZSM-5: On the Origin of the Olefinic Species. *J. Catal.* **2007**, *249* (2), 195.
(34) Tessonnier, J. P.; Louis, B.; Rigolet, S.; Ledoux, M. J.; Pham-Huu, C. Methane Dehydro-Aromatization on Mo/ZSM-5: About the Hidden Role of Brønsted Acid Sites. *Appl. Catal., A* **2008**, *336* (1−2), 79.
(35) Masiero, S. S.; Marcilio, N. R.; Perez-Lopez, O. W. Aromatization of Methane over Mo-Fe/ZSM-5 Catalysts. *Catal. Lett.* **2009**, *131* (1−2), 194.
(36) Ohnishi, R.; Ichikawa, M. Effect of CO_2/CO Addition in Dehydroaromatization of Methane on Zeolite-Supported Mo and Re Catalysts towards Hydrogen, Benzene and Naphthalene. *Catal. Surv. Jpn.* **2002**, *5* (2), 103.
(37) Bai, L.; Kudo, S.; Norinaga, K.; Wang, Y.; Hayashi, J. Kinetics and Mechanism of Steam Gasification of Char from Hydrothermally Treated Woody Biomass. *Energy Fuels* **2014**, *28* (11), 7133.
(38) Liu, S.; Ohnishi, R.; Ichikawa, M. Promotional Role of Water Added to Methane Feed on Catalytic Performance in the Methane Dehydroaromatization Reaction on Mo/HZSM-5 Catalyst. *J. Catal.* **2003**, *220* (1), 57.
(39) Chen, H.; Li, L.; Hu, J. Upgrading of stranded gas via non-oxidative conversion processes. *Catal. Today* **2017**, DOI: 10.1016/j.cattod.2017.05.029.
(40) Ma, H.; Kojima, R.; Ohnishi, R.; Ichikawa, M. Efficient Regeneration of Mo/HZSM-5 Catalyst by Using Air with NO in Methane Dehydro-Aromatization Reaction. *Appl. Catal., A* **2004**, *275* (1−2), 183.
(41) Won, W.; Lee, K. S.; Seo, S. Online Optimization of CATOFIN Process. In *ICCAS 2007 - International Conference on Control, Automation and Systems*, 2007; pp 250−255.
(42) Panditrao, S. "On-purpose Olefins through CATOFIN® -CATADIENE® Technologies". http://www.propylene-propane-markets-2014.com/media/downloads/16-day-two-sunil-panditrao-technology-manager-cbandi.pdf.
(43) Gao, J.; Zheng, Y.; Jehng, J.; Tang, Y.; Wachs, I. E.; Podkolzin, S. G. Identification of Molybdenum Oxide Nanostructures on Zeolites for Natural Gas Conversion. *Science* **2015**, *348* (6235), 686.
(44) Xu, Y.; Wang, J.; Suzuki, Y.; Zhang, Z. G. Effect of Transition Metal Additives on the Catalytic Stability of Mo/HZSM-5 in the Methane Dehydroaromatization under Periodic CH_4-H_2 Switch Operation at 1073 K. *Appl. Catal., A* **2011**, *409−410*, 181.
(45) Rodríguez-González, L.; Hermes, F.; Bertmer, M.; Rodríguez-Castellón, E.; Jiménez-López, A.; Simon, U. The Acid Properties of H-ZSM-5 as Studied by NH_3-TPD and ^{27}Al-MAS-NMR Spectroscopy. *Appl. Catal., A* **2007**, *328* (2), 174.

DOI: 10.1021/acs.iecr.7b05094
Ind. Eng. Chem. Res. 2018, 57, 4505−4513